Sci. Dril., 35, 39–53, 2026
https://doi.org/10.5194/sd-35-39-2026

Scientific Drilling
Open Access

Geochemical and structural indicators for hydrothermal fluid migration: a case study in the Bushveld Complex

Rolene Lubbe[1], **Amy J. Allwright**[2], **Stephanus S. de Lange**[1], **and Frederick Roelofse**[3]

[1]Institute for Groundwater Studies, University of the Free State, Bloemfontein, South Africa
[2]Department of Earth Sciences, Stellenbosch University, Stellenbosch, South Africa
[3]Department of Geology, University of the Free State, Bloemfontein, South Africa

Correspondence: Rolene Lubbe (rolenelubbe43@gmail.com)

Received: 20 June 2025 – Revised: 16 November 2025 – Accepted: 3 December 2025 – Published: 27 February 2026

Abstract. The Bushveld Complex is a renowned crystalline igneous intrusion, with various hypotheses regarding its origin. However, the role of post-magmatic hydrothermal fluids in its evolution remains underexplored. The present hydrogeological study, based on data derived from a deep exploration well drilled into the eastern limb of the Bushveld Complex as part of the Bushveld Complex Drilling Project (BVDP) funded by the International Continental Scientific Drilling Program (ICDP) and which intersects with a lamprophyre dyke at depth, highlights geochemical and structural indicators of deep-seated hydrothermal fluid migration within the crystalline formation. A distinct hydrogeochemical transition is observed at 450 m below ground level, coinciding with a severely fractured anorthosite layer, with evidence of mineral crystallisation from post-magmatic hydrothermal fluid migration. The zone is characterised by a significant increase in total dissolved solids (TDSs), sodium, chloride, sulfate, calcium, potassium, zinc, fluoride and boron concentrations, as well as elevated concentrations of redox-sensitive trace metals such as iron and manganese, in addition to stable isotope deviations. These signatures suggest hydrothermal fluid–rock interactions facilitated by structural conduits for fluid migration, such as dykes and fractured zones. The hydrogeological data and geological features suggest deep-seated, saline and potentially volatile-rich fluid migration, which has implications for post-magmatic hydrothermal mineralisation and groundwater evolution. The potential association of these fluids with volatiles poses exploration risks and highlights the need for integrated gas monitoring. Real-time drilling fluid analysis and isotopic characterisation are recommended to better elucidate fluid sources and migration pathways. These findings contribute to an updated understanding of post-magmatic processes using geochemical indicators to inform future exploration and groundwater management strategies in these fractured crystalline formations.

1 Introduction

1.1 Background

The Bushveld Complex contains the world's largest mafic to ultra-mafic layered intrusion, the Rustenburg Layered Suite (RLS), known for its mineral wealth and complex geological evolution and hydrothermal history (Cole et al., 2024; Harney and Von Gruenewaldt, 1995; Scoon and Viljoen, 2016). Most published articles regarding the proposed origin of the RLS of the Bushveld Complex focus on the idea that multiple pulses of magma were involved in its petrogenesis, although the sources of the magma are not widely agreed upon (Bilenker et al., 2017; Cole et al., 2024; Contreras et al., 2024; Zeh et al., 2015).

Hydrothermal fluid migration within the Bushveld Complex is strongly influenced by structural features such as dykes and fracture zones, which enhance permeability and therefore act as conduits for deep-seated fluid migration (Curewitz and Karson, 1997; Gudmundsson, 2022). These structures often host mineralised veins, as seen in quartz-bearing fractures in the Waterberg deposit, as well as hydrothermal pipes enriched with volatiles and ore minerals (Marsh et al., 2021; Vonopartis et al., 2020; Zhitova et al., 2016). Zaccarini and Garuti (2020) demonstrated that miner-

als such as zoned laurite in the Merensky Reef likely formed from direct interaction with or precipitation from hydrothermal fluids.

Hydrothermal alteration processes in the Bushveld Complex also correlate with increased salinity and volatile content in groundwater, indicating deep magmatic sources (Harney and Von Gruenewaldt, 1995; Marsh et al., 2021; Zhitova et al., 2016; Zhou et al., 2023). A deep exploration well that is currently being drilled into the eastern limb of the Bushveld Complex as part of the International Continental Scientific Drilling Program (ICDP) Bushveld Complex Drilling Project (BVDP) intersected a lamprophyre dyke at depth. Early indications suggest that this dyke may be acting as a conduit for the upward migration of deep-seated hydrothermally altered groundwater and associated volatiles, which migrate to the surface through fracture zones linked to possible groundwater flow. Geochemical anomalies and stable isotope deviations from typical meteoric signatures, notably showing enrichment of δ^2H and δ^{18}O in association with structural features at depth, suggest hydrothermal influence.

Understanding the structural and geochemical indicators of hydrothermal influence and migration in the Bushveld Complex is essential, given the potential for such deep-seated fluids to mobilise volatiles, such as methane. These findings inform exploration strategies and groundwater management in crystalline formations, advancing hypotheses regarding the genesis and post-emplacement evolution of the Bushveld Complex.

While the magmatic evolution and crystallisation of the Bushveld Complex, including its upper felsic units (the Rashoop Granophyre and Lebowa Granite suites), have been extensively studied (Skursch et al., 2024), the role of deep-seated hydrothermally altered fluids in the mafic to ultramafic sequence remains relatively underexplored, specifically, the hydrogeochemical signatures related to fluid migration governed by structural features such as fractures and dykes.

Research objectives

This study examines the geochemical and structural indicators of hydrothermal fluid migration within the Bushveld Complex, prompted by the detection of anomalous groundwater in a deep exploration well that intersects with a lamprophyre dyke at depth. The research focuses on assessing the role of structural features, such as fractures and dykes, as conduits for deep-seated fluid migration potentially associated with volatile species. Therefore, the objective is to determine whether the observed geochemical anomalies and stable isotope deviations suggest hydrothermal influence. The study aims to enhance our understanding of deep-seated fluid migration pathways and their role in fluid–rock interactions by linking these hydrogeochemical signatures to structural features within the RLS of the Bushveld Complex. Ultimately, the findings establish a foundation for future investigations involving real-time gas monitoring and isotopic techniques (e.g. δ^{13}C, ^{3}He / ^{4}He) to explain the origin and evolution of deep fluids and the volatiles that they carry within the Bushveld Complex.

1.2 Geological and hydrogeological setting

The Paleoproterozoic ($\sim$ 2.06 Ga), approximately 7 to 9 km thick, mafic to ultra-mafic RLS of the Bushveld Complex intrudes into the Kaapvaal Craton and appears to have been constructed through the repetitive influx of several compositionally distinct magmas (Cawthorn, 2006; Daya, 2019; Scoon and Viljoen, 2016). It occurs, exposed, in four limbs (the far western, western, northern, and eastern limbs) and hosts world-class deposits of platinum group elements (PGEs), chromium and vanadium (Cawthorn, 2006; Scoon and Viljoen, 2016; Skursch et al., 2024; Zientek et al., 2014) (Fig. 1).

The lower reaches of the RLS, the Lower and Lower Critical zones, are ultra-mafic in composition and dominated by peridotitic and pyroxenitic lithologies, with mafic compositions becoming more common in the Upper Critical, Main and Upper zones, which host an abundance of gabbroic, noritic and gabbronoritic rocks, in addition to lesser anorthositic, pyroxenitic and dioritic rocks (Cawthorn, 2006). These crystalline igneous rocks generally exhibit low primary porosity and permeability, suggesting that groundwater movement will be confined mainly to structural features such as fractures and dykes, along with associated weathered zones that act as conduits for fluid migration (Cook, 2020; Freeze and Cherry, 1979; Titus et al., 2009).

The Bushveld Complex hosts multiple aquifer systems, ranging from weathered aquifers and shallow perched aquifers in the weathered zone to deeper fractured bedrock aquifers, where groundwater flow diminishes with depth due to reduced fracture frequency (Gebrekristos and Cheshire, 2012; Titus et al., 2009). However, groundwater occurrence at depth is primarily governed by secondary porosity, which is linked to structural features (Titus et al., 2009).

2 Methodology

The present study is based on core drilling being conducted on the eastern limb of the RLS by the BVDP project of the ICDP (Fig. 1), with hydrogeological data collected to a depth of 950 m below ground level (m b.g.l.). The near-vertical well was collared in the Upper Critical zone of the RLS, between the UG1 and MG4 chromitite layers. Drilling was conducted in phases to facilitate systematic data collection during the survey periods.

In Phase 1, drilling progressed to 350 m b.g.l., followed by flushing operations for approximately 9 h to eliminate residual drilling fluids. A geophysical downhole survey was then performed over 2 d, including hydrogeological logging, which recorded the electrical conductivity (EC) with depth.

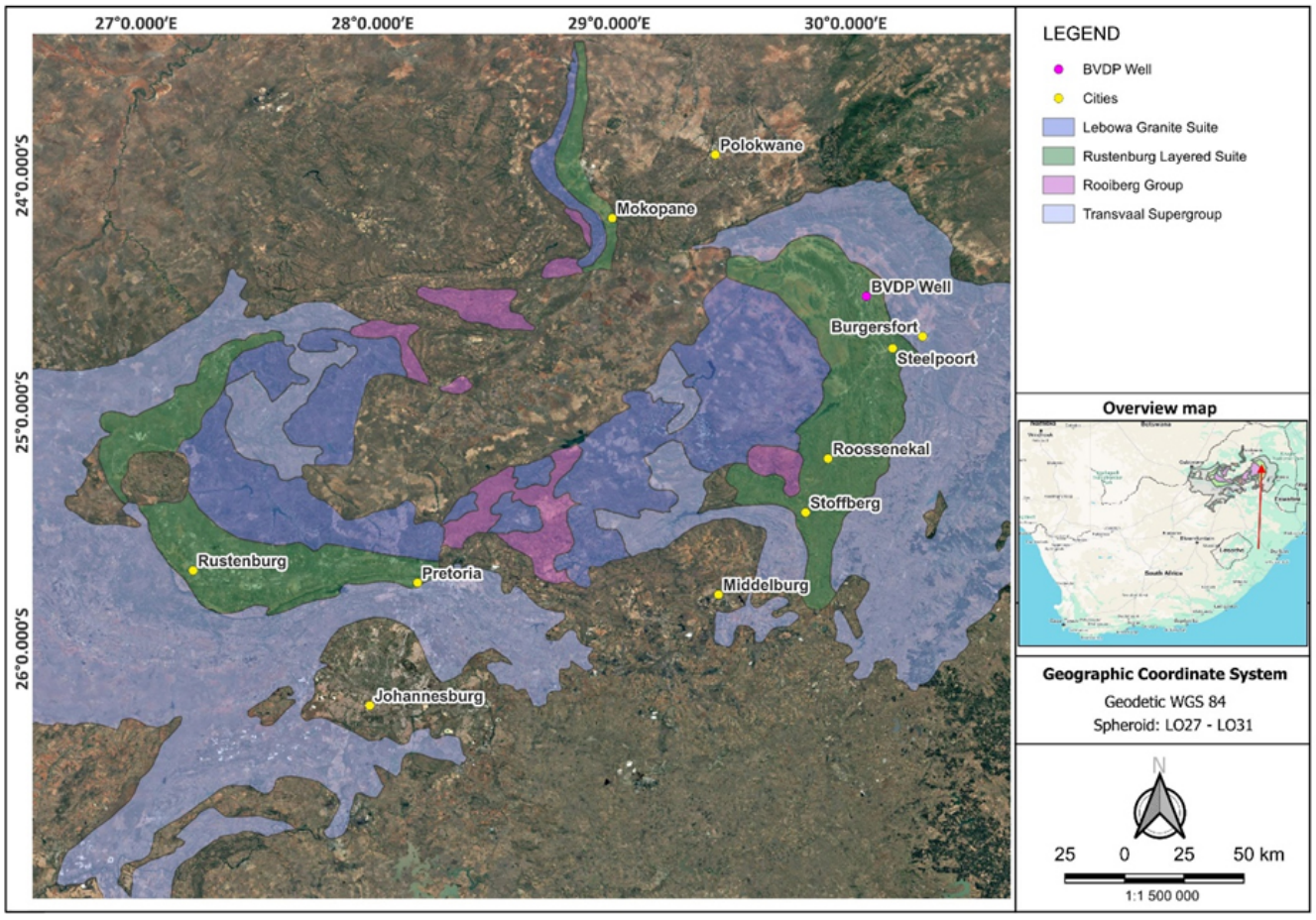

Figure 1. Map showing the distribution of the RLS of the Bushveld Complex and the location of the exploration well on which this study is based (adapted from Skursch et al., 2024).

This information aided in identifying intervals of elevated hydraulic conductivity, which were subsequently targeted for groundwater sampling and hydrogeological characterisation. Six depth-specific groundwater samples were collected using a controlled-depth sampler. Following the sampling, the well was cased and cemented to the bottom of this interval to minimise water loss and maintain its structural integrity.

Phase 2 extended the well from 350 to 950 m b.g.l. The same protocol was followed: flushing for approximately 9 h to displace drilling fluids, followed by a 3 d resting period while geophysical surveys and hydrogeological logging were conducted to delineate permeable zones. These zones were targeted for hydrogeological sampling at specific depths using a controlled-depth sampler, where 10 depth-specific groundwater samples were collected. After the survey, the well was cased and sealed with cement again to maintain structural integrity before proceeding with further drilling.

This study examines the lithological, hydrogeological, and hydrogeochemical data obtained from Phases 1 and 2 of the drilling. Lithological logs were utilised to identify zones likely to exhibit higher permeability due to weathering and fracturing caused by faults and intrusive features. These features were confirmed by hydrogeological profiles and targeted for groundwater sampling. Phase 3, which will extend drilling from 950 to ∼2000 m b.g.l., revealed anomalous groundwater influx between ∼1150 and ∼1270 m b.g.l. during cementation, attributed to persistent fluid movement; however, analysis from this interval falls outside the scope of this paper. The lithological data for Phase 3 have been incorporated into this report; however, the water quality analysis, isotope analysis and hydrogeological profile data for Phase 3 are currently unavailable.

Depth-specific groundwater samples collected during Phases 1 and 2 underwent chemical and isotopic analyses. The samples were collected in duplicate in sterile 500 mL plastic bottles. One unfiltered sample was retained for chemical analysis. The second sample was filtered through a 0.45 µm syringe filter for stable isotope analysis and transferred into sterile 100 mL glass bottles. Field parameters, including pH, EC, temperature, redox potential and dissolved oxygen, were measured at the time of sampling using cal-

ibrated field instruments. Strict contamination control procedures were followed, including the use of plastic gloves throughout all stages of filtering and sample handling. Samples were filled to eliminate headspace and then were labelled and stored.

Accredited laboratories analysed the depth-specific groundwater samples. Chemical analysis included major cations, anions and trace elements. The analysis was conducted utilising methodologies such as inductively coupled plasma mass spectrometry (ICP-MS) and inductively coupled plasma optical emission spectroscopy (ICP-OES).

The water samples were analysed for their chemical content, including trace elements and heavy elements, using a Teledyne Leeman Prodigy 7 ICP-OES with a Meinhard nebuliser and a long-neck cyclonic spray chamber. Certified reference materials (standards and quality checks), obtained from De Bruyn Spectroscopic Solutions, an ISO 17025-accredited supplier, were used for calibration and quality control of the ICP-OES (RMP004).

Stable isotopes included $\delta^{18}O$ and $\delta^{2}H$ ratios. The methods used included isotope ratio mass spectrometry (IRMS) and laser-based spectroscopy (Los Gatos Research (LGR)/Picarro cavity ring-down spectroscopy (CRDS)).

IRMS was preferentially used for the depth-specific samples due to its lower sensitivity to organic contamination. It is described as a preferred method when dealing with contaminated or complex samples where organics are expected as the conversion process effectively removes many impurities. IRMS is a method for analysing the isotopic abundances of light elements, including carbon, hydrogen, oxygen, sulfur and nitrogen (Muccio and Jackson, 2009). It relies on a multi-collector magnetic sector mass spectrometer for high sensitivity and precision in detecting isotopic variations (Muccio and Jackson, 2009). The instrument includes a sample introduction system, an electron ionisation source, a magnetic sector analyser, a Faraday collector detector array and a data acquisition system (Muccio and Jackson, 2009). Samples are ionised, and the magnetic sector separates ions by their mass-to-charge ratio. The multi-collector detector array then measures the various isotopes simultaneously, determining their ratios relative to isotopic standards (Muccio and Jackson, 2009).

The Picarro system was used for the Phase-2 depth-specific groundwater samples as these samples exhibited visible signs of drilling fluid contamination. While it is easier to operate and maintain with simpler sample preparation compared to IRMS, the Picarro system is more sensitive to organic interference than IRMS. The IRMS has a lower sensitivity to organic contamination due to its chemical conversion process, which removes many impurities and maintains high precision even with contaminated samples. Despite IRMS being recognised as superior for contaminated samples, the Picarro system was the primary method employed for Phase-2 samples, likely due to logistical or cost considerations, as the expense of running the IRMS for a small number of samples posed a hurdle. For samples analysed by Picarro when organic compounds are present, pretreatment, sample purification or the application of multiple analysis methods may be necessary to ensure accurate results. To mitigate the effects of residual drilling fluid contamination on the Phase-2 samples analysed by Picarro, they were allowed time to settle. They were filtered a second time to remove as much of the residual drilling fluid as possible. This filtering process was often complex due to the viscous nature of some samples, resulting from the drilling fluids, and sometimes required multiple filters. These steps aimed to ensure that the samples were as clean as possible for the Picarro analysis.

Picarro instruments employ CRDS, a technique that draws a sample (usually air or gas) into a controlled cavity (Mouat et al., 2024). A laser beam is directed into the cavity, reflecting off mirrors to create a lengthy optical path. When the laser is switched off, a photodetector measures the rate of decay in light intensity. A quicker decay rate indicates greater absorption by the target substance. By adjusting the laser to known absorption wavelengths, the instrument can determine concentrations of gas species or quantify isotope ratios such as $\delta^{18}O$ and $\delta^{2}H$ (Mouat et al., 2024).

3 Results and discussion

3.1 Lithological logs and hydrogeological features

The upper 500 m of the BVDP well intersected rocks of the Upper Critical zone of the RLS, including norites, gabbronorites, anorthosites, pyroxenites, chromitites and minor serpentinites. Several dolerite layers were also intersected across this interval. The first chromitite layer, the MG4 chromitite, was intersected at a depth of ∼ 255 m b.g.l., with the MG3 chromitite following at a depth of ∼ 495 m b.g.l. The MG2 chromitite, being the first chromitite belonging to the Lower Critical zone, was intersected at a depth of ∼ 504 m b.g.l. The ensuing sequence of rocks belonging to the Lower Critical zone is dominated by ultra-mafic lithologies including harzburgite, dunite and a variety of pyroxenites. The lowermost chromitite horizon of the RLS, the LG1 chromitite, was intersected at a depth of ∼ 810 m b.g.l. At the time of writing, the well extended down to a depth of ∼ 1270 m b.g.l., within a lamprophyre dyke intersected at ∼ 1267 m b.g.l.

The rocks of the Upper Critical zone are characterised by low primary porosity due to their crystalline nature. However, fracturing within these units enhances secondary porosity, thereby increasing their permeability and the potential for fluid flow. These fractures range from ∼ 100 to ∼ 500 m b.g.l., which represents the shallow to intermediate aquifer. The presence of these fractures can be observed in the lithological logs and hydrological data (Fig. 2). Additionally, the presence of serpentinite suggests hydrothermal

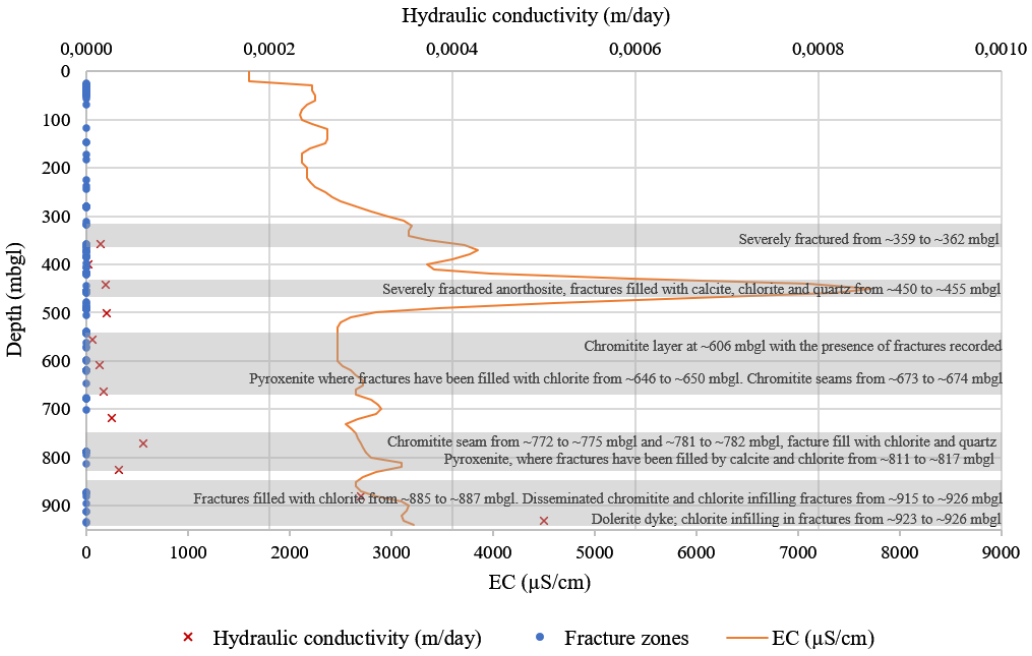

Figure 2. Correlation of the hydraulic conductivity of potential fracture zones as determined from the packer test with the hydrogeological logging (EC profile), as well as potential fracture zones determined from structural logs based on geophysical survey data, in addition to the lithological log descriptions.

alteration, which may further enhance fracture permeability and fluid transport capacity.

Within this interval, open fractures were identified at depths of up to 322 m b.g.l. The presence of these extensive shallow fractures resulted in total water loss during drilling until the upper 350 m of the well was sealed, indicating high permeability in the shallow subsurface. While most fractures within this broader range may contain infill materials such as calcite and chlorite, open fractures in the upper section facilitate considerable fluid flow (Fig. 2).

A severely fractured anorthosite layer hosting disseminated chromitite was encountered between ~450 and ~455 m b.g.l. (Fig. 2). Fractures within the anorthosite were filled by calcite, chlorite and quartz, which may be indicative of past hydrothermal fluid circulation (Setera et al., 2023).

A high-density fractured zone was intersected at ~800 m b.g.l., extending deeper as indicated by lithological and hydrological logging data in Fig. 2, which challenges conventional assumptions regarding the low permeability of unweathered igneous rock at such depths. It provides clear evidence that deep-seated fractures and structural discontinuities serve as key conduits for groundwater movement even within otherwise low-permeability crystalline formations. While hydraulic conductivity values obtained from packer tests in this deep interval were generally lower than those in shallow zones, they did exhibit variations, with slightly higher values correlating to specific geological features, such as disseminated chromitite and chlorite infilling fractures between ~915 and ~926 m b.g.l. and severely fractured zones with chloritic infilling around 885 to 887 m b.g.l. (Fig. 2). These findings underscore the importance of structural features in controlling permeability at depth. The high fracture density in the ~800 to ~935 m b.g.l. interval suggests the potential for localised deep aquifer systems.

The geophysical dataset provides a powerful analytical perspective on the structural controls that govern groundwater movement within the crystalline formations of the Bushveld Complex. Given that groundwater movement in these inherently low-primary-porosity rocks is primarily confined to structural features such as fractures and dykes, these geophysical tools are essential for identifying potential fluid pathways. Acoustic Televiewer (ATV) imaging effectively reveals features such as fractures and textural differences on the well wall (Wedge et al., 2017). The variations in signal return, shorter in compact, intact areas and longer or more scattered in fractured or enlarged regions, visually emphasise the existence of open structures likely functioning as fluid flow conduits (Wedge et al., 2017). These images provide a clear view of unique patterns that reveal hydraulically significant intervals at various depths: ~360 m b.g.l., which aligns with the lithological log of a highly fractured zone between ~359 and ~362 m b.g.l.; around 450 m b.g.l., where severely fractured anorthosite layers exhibit calcite, chlorite and quartz infilling; ~606 m b.g.l., where a chromitite layer with fractures is noted; from ~646 to ~650 m b.g.l., where pyroxenite fractures have been documented with chlorite infillings; ~885 m b.g.l., where fractures are recorded with chlorite in-

filling; and ∼ 932 m b.g.l., which is close to the dolerite dyke, where fractures have chloritic infilling.

Caliper data add a significant perspective to this analysis. Whether gathered from a standard three-arm tool or derived from logging-while-drilling (LWD) density measurements, fluctuations in well diameter can serve as indicators (Liu et al., 2019; Montone et al., 2024). Increases in both minimum and maximum diameter measurements often signal areas of mechanical weakness or open fracturing, characteristics that frequently correspond with observed hydrological responses (Crow et al., 2013). This provides objective evidence of physically open spaces within the rock mass that facilitate fluid movement, as seen at approximately 360 m b.g.l., corresponding with the lithological log of a highly fractured zone between ∼ 359 and ∼ 362 m b.g.l. At around 450 m b.g.l., severely fractured anorthosite layers show calcite, chlorite and quartz infillings. At approximately 606 m b.g.l., a chromitite layer with noted fractures is observed, and at ∼ 932 m b.g.l., near a dolerite dyke, fractures are filled with chlorite.

While not a direct geophysical instrument, Rock Quality Designation (RQD) provides valuable supplementary insights (Hasan et al., 2022). Typically, low RQD values are linked with fractured or weathered sections (Hasan et al., 2022), mirroring patterns observed in the ATV and caliper logs at depths of approximately 360, 450, 492, 606 and 788 m b.g.l. These disrupted areas, defined by heightened secondary porosity and permeability, often exhibit the greatest reactivity during hydraulic testing.

Collectively, the convergence of evidence obtained from imaging, mechanical logging and core-derived parameters indicates the presence of a coherent structural control on flow. In these contexts, features such as fractures and dykes are not merely incidental; rather, they represent the primary pathways through which groundwater moves.

Drilling operations below 950 m b.g.l. encountered further significant anomalies. During Phase-3 drilling, which will extend down to approximately 2000 m b.g.l., anomalous groundwater influx was observed between approximately ∼ 1150 and ∼ 1270 m b.g.l. This influx was substantial enough to cause difficulties with well construction. A significant challenge was the inability to successfully cement the well between ∼ 1150 and ∼ 1270 m b.g.l., despite four attempts. This persistent failure to cure the cement was directly attributed to significant groundwater inflows within this zone, indicating active water movement through fractures or permeable zones at these depths. Visual evidence from the re-drilled cement core distinctly shows areas where flow prevented the cement from setting (Fig. 3).

The well at this depth interval intersected with a lamprophyre dyke at approximately 1267 m b.g.l., which exhibited significant fracturing and weathering. The lamprophyre dyke and associated structural features in this deep zone are interpreted as significant conduits for fluid flow.

Figure 3. Re-drilled cement core (diameter of ∼ 50 mm) from the depth interval of approximately ∼ 1150 to ∼ 1270 m b.g.l. The distinct places where fluid flow prevented the cement from curing provide visual evidence of significant groundwater inflows and active water movement through fractures or permeable zones at these depths (photograph taken by Pieter Frederik Grobler).

Overall, the lithological sequence (Fig. 4) reflects a complex hydrogeological profile characterised by dense, low-permeability rocks interspersed with fractured dykes and weathered zones. Fluid flow is, therefore, likely to be constrained to structurally compromised zones where fracturing, faulting or intrusive events have generated secondary porosity. The physical features of the lamprophyre dyke suggest that it could act as a conduit for deep fluid migration, reinforcing the importance of structural controls on groundwater occurrence in crystalline formations.

The presence of lamprophyres within the Bushveld Complex is well-documented (Daya, 2019; Hughes et al., 2016; Krmíček and Chalapathi Rao, 2022; Stemprok and Seifert, 2011). These intrusions typically appear as dykes or isolated pockets emplaced into the felsic and mafic rocks of the Bushveld Complex and are classified as alkaline lamprophyres (Daya, 2019). Lamprophyres form from mantle-derived melts within subduction zones and continental rift settings (Stemprok and Seifert, 2011). They are known to transport high-temperature, volatile-rich fluids from the mantle, thereby making them potential conduits for mantle-sourced volatiles and deep fluid flow within the crust

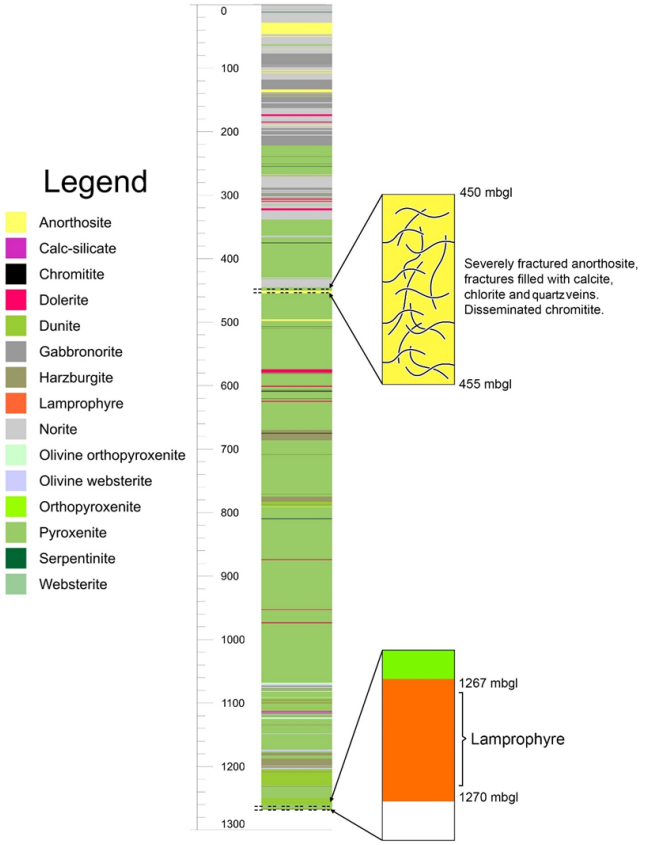

Figure 4. Lithological log of the BVDP well on the eastern limb of the RLS down to a depth of ~1270 m b.g.l. Mafic rocks dominate the Upper Critical zone sequence, intersected down to a depth of 500 m b.g.l., with the Lower Critical zone consisting of ultramafic rocks. Between ~450 and ~455 m b.g.l., a severely fractured anorthosite layer was intersected, demonstrating evidence of potential hydrothermal alteration through fractures filled with calcite, chlorite and quartz. A lamprophyre dyke was intersected at a depth of ~1267 m b.g.l.

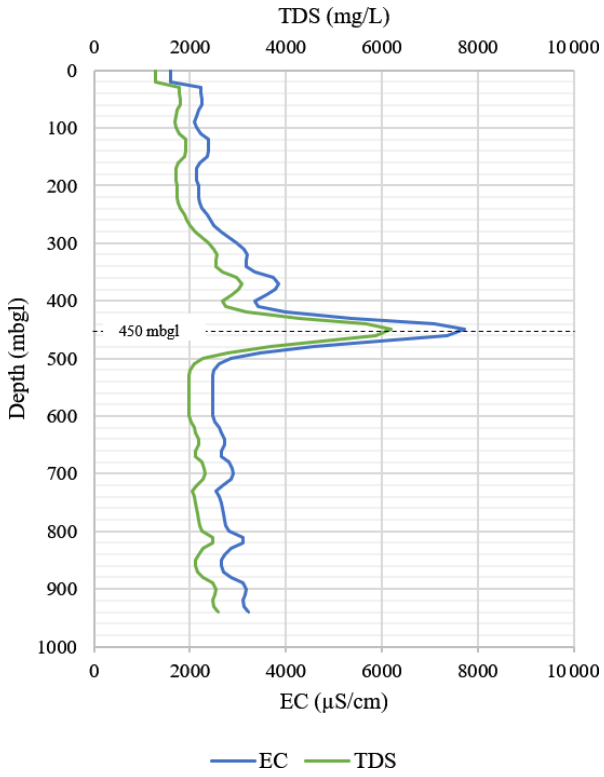

Figure 5. Variation in TDS with depth in the BVDP well. TDS was derived from the measured EC obtained through down-hole hydrogeological logging (a factor of 0.8 was used for the conversion for deep groundwater). A significant spike in TDS is observed at 450 m b.g.l.

(Stemprok and Seifert, 2011). Their occurrence within the Bushveld Complex has significant implications for understanding deep hydrogeological processes and the potential mobilisation of mantle-derived fluids into the upper crust.

3.2 Hydrogeological logging

The downhole hydrogeological logging recorded continuous EC as a function of depth, which was subsequently used to calculate total dissolved solid (TDS) concentrations. These TDS values served as indicators for identifying potential zones of groundwater ingress into the crystalline rocks of the RLS.

The TDS profile revealed a series of distinct peaks with depth, suggesting discrete zones of elevated salinity potentially linked to active or historic groundwater ingress (Fig. 5). These anomalies guided depth-specific groundwater sampling. A general increase in TDS with depth was observed, consistent with trends reported for deep crystalline aquifers, where longer residence times, fluid–rock interaction and restricted circulation contribute to increased salinity (Boumaiza et al., 2024).

The most significant anomaly occurred between 450 and 455 m b.g.l., where TDS exceeded 6000 mg L^{-1}, as displayed in Fig. 5. This distinct peak is indicative of highly saline or mineralised groundwater and coincides with a zone of intense fracturing and mineral crystallisation in fractures within an anorthosite layer. Together with the geological observations, the TDS signature suggests that this fractured zone may act as a conduit for deep-seated, evolved fluids, potentially of hydrothermal origin, within an otherwise low-permeability crystalline formation.

3.3 Hydrogeological samples

Depth-specific groundwater samples were collected during Phases 1 and 2 of the survey, with sampling depths informed by lithological logs and hydrogeological down-hole profile data. These samples were analysed for their chemical composition and stable isotopic signatures. The chemical anal-

ysis encompassed the determination of anions, cations and trace elements.

A Piper diagram serves as a hydrogeochemistry tool for analysing results. It visualises hydrogeochemical data, categorises samples and infers reactions based on subsurface composition. The diagram illustrates the concentrations of major cations (calcium, magnesium, sodium, potassium) and anions (chloride, bicarbonate, sulfate) in milliequivalent percentages across two triangular representations (Kumar, 2013). Data from these triangles extend into a central diamond shape, which reflects the overall characteristics or type of the groundwater sample (Kumar, 2013).

The Phase-1 (shallower) groundwater samples exhibit a mixed (Mg–Ca–Cl–HCO_3) water type, as displayed in Fig. 6. In contrast, the Phase-2 (deeper) groundwater samples predominantly show a sodium chloride (Na–Cl) water type, except for the sample collected at 450 m b.g.l., which is characterised by a calcium chloride (Ca–Cl) water type (Fig. 7). The sample from 450 m b.g.l. is likely to be representative of a transition zone between the shallower mixed (Mg–Ca–Cl–HCO_3) water type and the deeper sodium chloride (Na–Cl) type. This transition is supported by the down-hole hydrogeological profile data, which reveal a spike in TDS concentration at this depth, coinciding with the fractured anorthosite layer – a feature that is likely to be indicative of hydrothermal activity (Setera et al., 2023). Forrest et al. (2013) similarly describe hydrothermal systems as typically being associated with sodium chloride waters.

The observed change in geochemical composition with depth aligns with trends noted by Boumaiza et al. (2024), where groundwater in crystalline formations tends to shift toward calcium chloride or sodium chloride water types as depth increases. As groundwater salinity rises, sulfate concentrations also increase, often reaching brine levels (TDS $> 10\,000\,mg\,L^{-1}$), indicating a transition to reducing environments (Boumaiza et al., 2024). This trend reflects the general geochemical evolution of groundwater, transitioning from an Mg–HCO_3 / SO_4 water type in shallow zones to a Ca / Na–Cl water type at greater depths (Boumaiza et al., 2024; Freeze and Cherry, 1979). In the study area, the groundwater adheres to this typical geochemical pattern until it encounters saline groundwater, commonly attributed to old, deeply circulating fluids (Freeze and Cherry, 1979).

The Phase-1 and Phase-2 depth-specific groundwater samples were analysed for stable isotopes. The results were plotted against the Global Meteoric Water Line (GMWL) (Craig, 1961) and the Local Meteoric Water Line (LMWL) of Thohoyandou, Limpopo Province (Durowoju, 2019), as shown in Fig. 8. This isotopic analysis helped determine the origin of the groundwater and estimate its relative age by examining variations in heavy and light isotope species (Ortega and Gil, 2019). The isotopic data reveal two distinct groupings: the shallower Phase-1 samples correspond to groundwater that has been recently recharged by local precipitation. The Phase-2 samples, shallower than 450 m b.g.l., plot similarly to the Phase-1 samples, indicating a comparable origin. In contrast, the Phase-2 samples collected deeper than 450 m b.g.l. show a significantly more positive $\delta^{18}O$ signature, suggesting that these deeper samples result from prolonged water–rock interactions, leading to the development of saline "formation waters". This is particularly evident given the severely fractured anorthosite layer between 450 and 455 m b.g.l., as noted in the lithological logs. The term "formation waters", as defined by Pohl (2011), refers to groundwater of uncertain origin and age, often showing an increase in $\delta^{18}O$ with depth, which indicates potential hydrothermal influence. Furthermore, studies of the Canadian Shield's crystalline formations have demonstrated that deeper brines (< 1500 m b.g.l.) are generally more enriched in $\delta^{2}H$ compared to shallower brines. This observation aligns with the positive $\delta^{2}H$ values in the deeper Phase-2 samples, thereby further supporting the hypothesis of deep saline groundwater (Boumaiza et al., 2024).

3.4 Updated hydrogeological model

The recent geological and hydrogeological findings from the drilled exploration well in the eastern Bushveld Complex have led to an updated hydrogeological model, as illustrated in Fig. 9. The traditional hydrogeological conceptual model specifically focused on shallow groundwater (maximum depth of < 300 m b.g.l.), with fracture frequency decreasing with depth (Titus et al., 2009). In contrast, the updated hydrogeological conceptual model offers deeper insights that challenge the traditional conceptual model for crystalline formations. The revised conceptual model incorporates several key refinements, including a detailed assessment of the deeper fractured aquifers beneath the weathered zone. These fractures, which range in depth from ~ 100 to ~ 500 m b.g.l., are likely to facilitate preferential flow. Furthermore, the high-density fractured zone, located ~ 800 m b.g.l. and extending deeper into the Critical and Lower zones, is identified as an important pathway for groundwater movement. Significant groundwater anomalies were observed between ~ 1150 and ~ 1270 m b.g.l., where considerable groundwater inflow occurred, as evidenced by the persistent failure to cure the cement, which was directly attributed to significant groundwater inflows within this zone (Fig. 3). Structural features, such as the lamprophyre dyke intersected at ~ 1267 m b.g.l., are interpreted as fluid conduits in these deeper zones. The lamprophyre dyke is likely to be hydraulically connected to regional fault systems, facilitating the upward migration of fluid from deep-seated hydrothermal sources, potentially associated with volatile-rich saline or brine waters.

This updated understanding of the hydrogeological model in the Bushveld Complex is crucial for advancing scientific research. It enhances our knowledge of the geochemical evolution across the region, informs assessments of the hydrothermal potential for geothermal energy exploitation, and

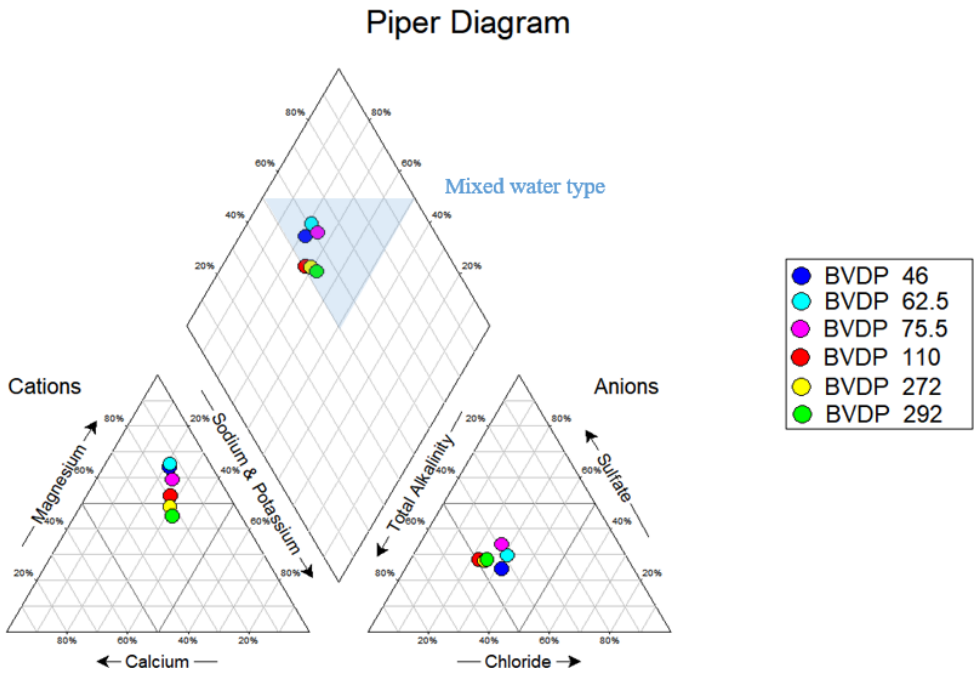

Figure 6. The Piper diagram of the Phase-1 depth-specific groundwater samples indicates an overall mixed water type.

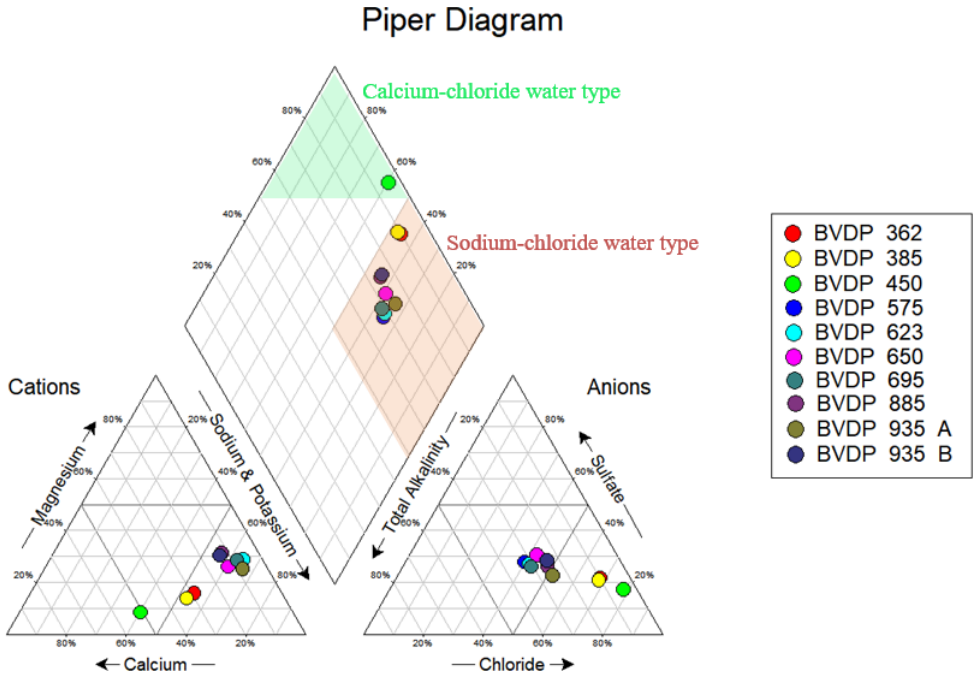

Figure 7. The Piper diagram for the Phase-2 depth-specific groundwater samples indicates an overall sodium chloride water type, except for the sample collected at 450 m b.g.l., which is characterised as a calcium chloride water type.

deepens our understanding of deep groundwater systems and their associated volatiles (Boumaiza et al., 2024).

3.5 Evidence of hydrothermal influence

A distinct geochemical and mineralogical anomaly was observed in groundwater collected at 450 m b.g.l. This sample was associated with a severely fractured anorthosite layer, where mineralised fracture fill comprised calcite, chlorite and

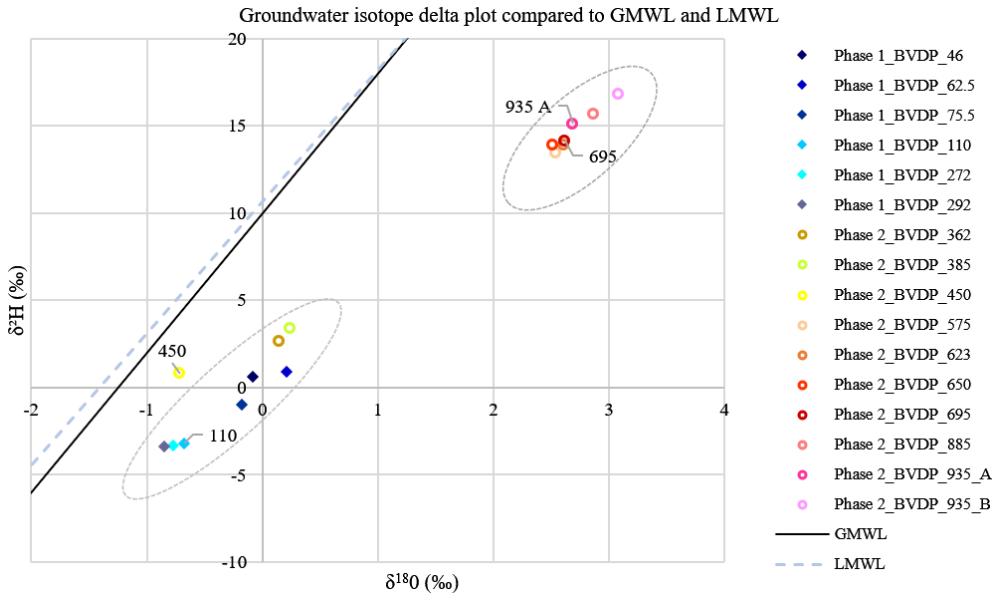

Figure 8. The distribution of the Phase-1 and Phase-2 depth-specific groundwater samples based on stable isotope analysis. Duplicate samples were collected for the samples at 935 m b.g.l. Every groundwater sample is positioned to the right of the GMWL ($\delta^2H = 8\delta^{18}O + 10$) (Craig, 1961) and the LMWL ($\delta^2H = 7.56\delta^{18}O + 10.64$) as defined for groundwater in Thohoyandou, Limpopo Province, by Durowoju (2019). The plot reveals two distinct groupings of the data: samples taken at depths shallower than 450 m b.g.l. and those taken at depths deeper than 450 m b.g.l. The sample at 450 m b.g.l. has a distinct isotopic plot, being isolated from the samples shallower than 450 m b.g.l.

quartz. These observations prompted further investigation into the possibility of hydrothermal influence at this depth.

Boumaiza et al. (2024) provide a helpful analogue from the Canadian Shield, a crystalline formation similar in terms of lithology and hydrogeological characteristics to the Bushveld Complex. Both regions are dominated by igneous units with negligible primary porosity, where groundwater movement is controlled by secondary porosity in fractured zones. In the Canadian Shield, shallow groundwater typically exhibits a calcium–sodium bicarbonate composition, indicative of recent meteoric recharge. In contrast, deeper systems (> 1000 m b.g.l.) exhibit calcium–sodium chloride compositions, characteristic of older, more evolved waters that have undergone prolonged water–rock interaction (Boumaiza et al., 2024).

In the Canadian Shield study, salinity and sulfate concentrations increased with depth, peaking at a TDS of 6000 mg L^{-1} at 780 m b.g.l., followed by a decline due to solubility constraints under reducing conditions (Boumaiza et al., 2024). Elevated iron and manganese concentrations were attributed to the dissolution of minerals and a reduction in oxidised phases (Boumaiza et al., 2024). Importantly, Boumaiza et al. (2024) linked these geochemical patterns to brine systems isolated from shallow groundwater flow, suggesting that these were hydrothermal fluids mobilised or altered during mining and drilling activities. The mineral precipitation of calcite and the presence of reducing conditions were noted as strong indicators of hydrothermal environments (Boumaiza et al., 2024).

In the current study, a TDS spike of 6000 mg L^{-1} at 450 m b.g.l. was similarly associated with elevated concentrations of sodium, chloride, sulfate, calcium, potassium, zinc and boron in the Bushveld Complex. These peaks were observed in a zone of intense fracturing and secondary mineralisation, suggesting a structurally controlled inflow of saline fluids. This is consistent with the mechanisms proposed by Boumaiza et al. (2024), which involve fractured crystalline formations intersecting with deep-seated hydrothermal brines.

Further evidence comes from the geochemical profiles shown in Figs. 10 and 11. TDS, sodium, chloride, sulfate, calcium, potassium and zinc all peak sharply at 450 m b.g.l. Boron and fluoride, both associated with hydrothermal systems (Forrest et al., 2013), also increase at this depth. Iron concentrations spike at 450 m b.g.l. and again at 695 m b.g.l., with manganese increasing progressively beyond 450 m b.g.l. These redox-sensitive elements indicate increasingly reducing conditions with depth, which aligns with the evolution of hydrothermal fluids.

Zhitova et al. (2016) reported similar saline, volatile-rich fluids in the Bushveld Complex based on fluid inclusion analysis. These fluids were enriched in sodium, potassium, calcium, chloride, iron, manganese and sulfate and were associated with thermally altered zones enriched in volatiles such as H_2O, CO_2 and CH_4. These volatiles play a central role in mineral transport and deposition under hydrothermal regimes (Zhitova et al., 2016).

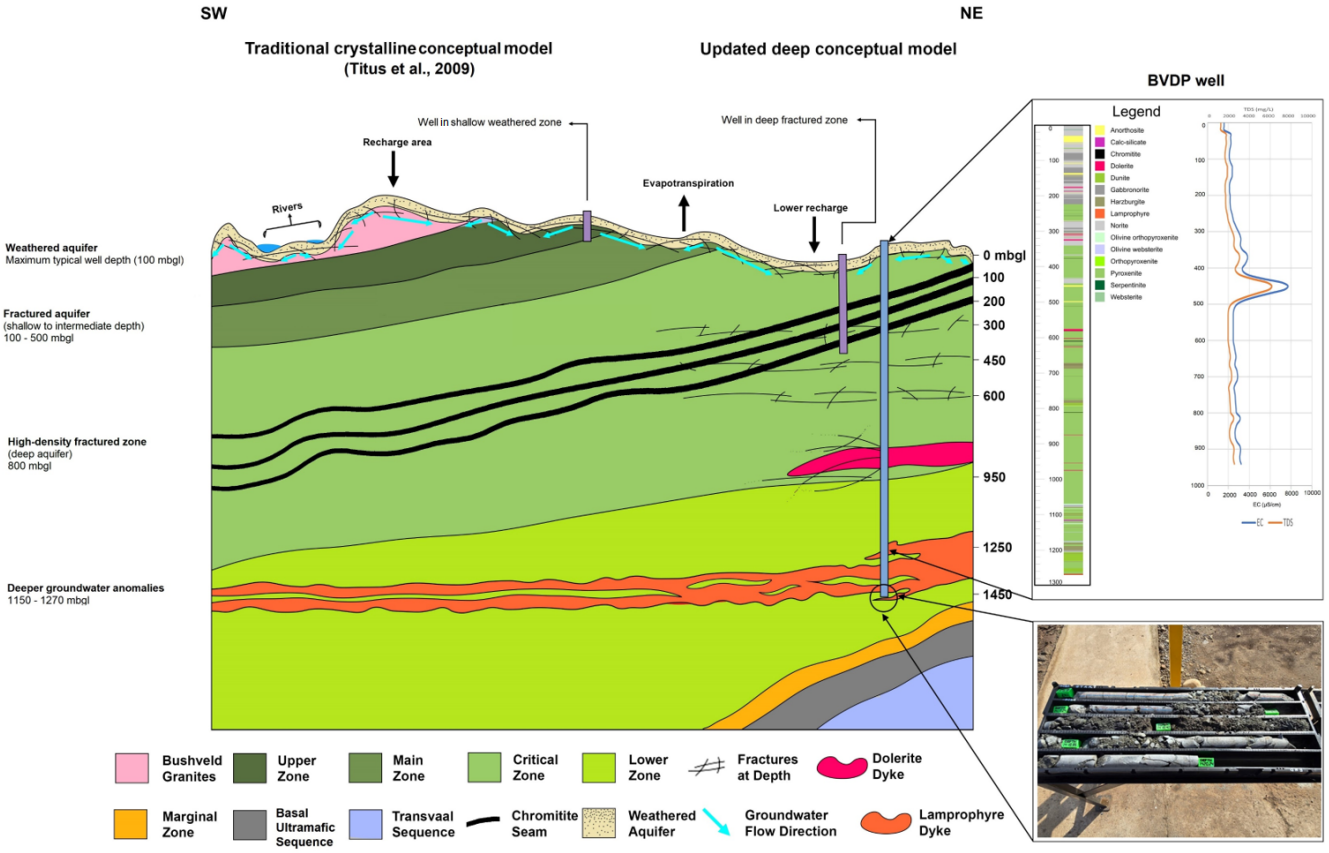

Figure 9. The updated hydrogeological conceptual model of the Bushveld Complex includes several aquifer systems in association with the lithological units of the Complex as compared to the traditional hydrogeological model (Titus et al., 2009). Weathered aquifers exist in the shallow weathered zone, where perched aquifers may have a hydraulic connection to rivers. Deeper fractured aquifers have fractures extending between ~ 100 and ~ 500 m b.g.l., with a high-density fractured zone at ~ 800 m b.g.l. Deeper groundwater anomalies are observed from ~ 1150 to ~ 1270 m b.g.l., likely to be correlated with the lamprophyric dyke encountered at ~ 1267 m b.g.l., as shown by the core image in the bottom-right corner. The two figures to the right show Figs. 4 and 5 in relation to the updated hydrogeological conceptual model.

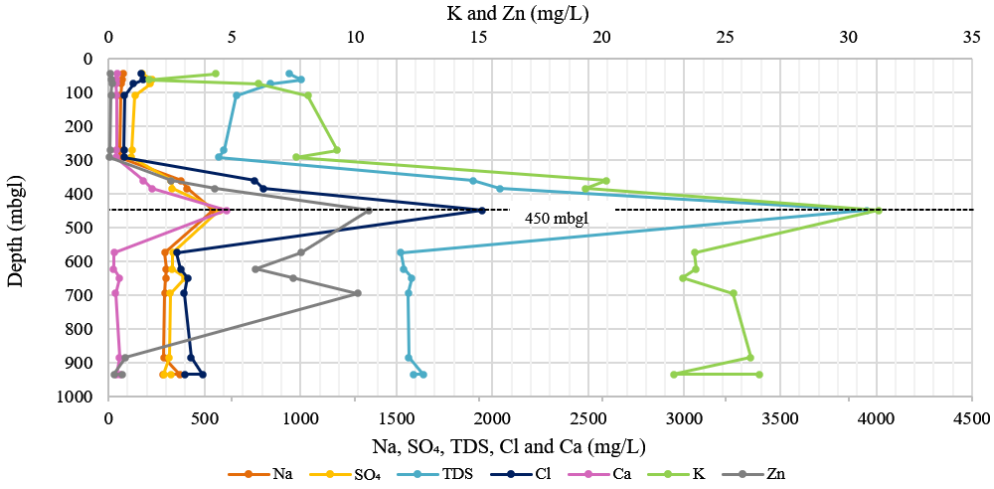

Figure 10. The graph displays the chemical parameters (sodium, sulfate, TDS, chloride, calcium, potassium and zinc) with increasing depth of the deep exploration well. The highest concentrations of these chemical parameters are measured at a depth of 450 m b.g.l.

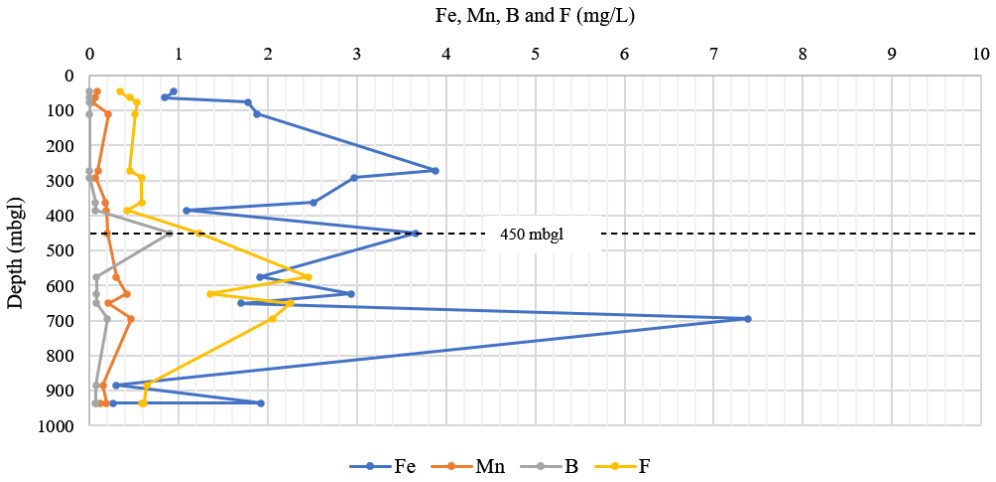

Figure 11. The graph displays the chemical parameters (iron, manganese, boron and fluoride) with increasing depth of the deep exploration well. Iron concentration increases significantly at 272, 450 and 695 m b.g.l., with the highest concentration being measured at 695 m b.g.l. The manganese and fluoride concentrations increase significantly from 450 m b.g.l. The highest concentration of boron is observed at 450 m b.g.l., after which the concentration decreases with depth.

The presence of a lamprophyre dyke intersected at ~ 1267 m b.g.l. in this study adds further weight to the potential hydrothermal fluid flow hypothesis. Dykes are known conduits for the migration of deep fluids and volatiles (Cook, 1998; Henry and Brovko, 2014; Stemprok and Seifert, 2011). Daya (2019) documented methane emissions in the western limb of the Bushveld Complex, which were associated with a lamprophyre dyke, suggesting deep-seated volatile migration along structural pathways. Reports from the mine in the current study area also noted the presence of methane, further supporting this interpretation. Sherwood Lollar et al. (2006) linked such methane occurrences in South Africa to Na–Ca–Cl- or Ca–Na–Cl-rich groundwater, suggesting an abiogenic origin.

Therefore, the geochemical and mineralogical evidence at 450 m b.g.l., including elevated salinity, redox-sensitive elements, boron enrichment and mineralised fractures, aligns with signatures of hydrothermal systems described in local and international studies. The structural features, particularly the severely fractured anorthosite and deep-seated lamprophyre dyke, likely facilitated the migration of hydrothermal brines enriched in major ions and volatiles. These fluids, isolated from shallow meteoric recharge, are inferred to be remnants of deep, reducing hydrothermal systems disturbed and mobilised during drilling.

Thus, if methane gas were to be present in the study area, as the mine reported, the presence of potential hydrothermal systems and groundwater chemistry at depth suggests a potential abiogenic origin (Brown, 1992).

4 Conclusion and recommendations

This study highlights the role of structural features, particularly deep-seated fractures and intrusive dykes, in facilitating the migration of potential hydrothermal fluids within the Bushveld Complex. Geochemical signatures observed at 450 m b.g.l., including elevated salinity, redox-sensitive elements and boron enrichment, provide robust evidence of potential hydrothermal influence. These fluids are viewed as saline, volatile-rich endmembers of deep-seated groundwater systems, isolated from shallow meteoric recharge and mobilised along structural conduits such as lamprophyre dykes. They are encountered at shallower depths through fractured features, including fractured anorthosites.

Hydrothermal fluids are important for the Bushveld Complex's mineral exploration and resource management. These fluids contribute to ore-forming processes and may also carry volatiles, such as methane, that pose operational and safety challenges during drilling. Understanding the geochemical and structural indicators of hydrothermal systems is crucial for guiding exploration projects and mitigating associated risks.

Beyond resource considerations, this study contributes to a broader understanding of deep crystalline aquifers, particularly the evolution and geochemical nature of saline groundwater within layered ultra-mafic to mafic intrusions. The results underscore the complexity of fluid–rock interactions at depth and suggest that volatiles associated with hydrothermal fluids may be more widespread in the Bushveld Complex than previously recognised.

Given the observed geochemical evidence and known volatile occurrences, it is recommended that real-time gas monitoring be integrated into exploration drilling campaigns in the Bushveld Complex. Portable mass spectrometers can

provide continuous in situ analysis of gases released during drilling via the circulating drilling fluid, as demonstrated by Erzinger et al. (2006). These data can reveal the presence, composition and concentration of deep-seated gases such as CH_4, CO_2 and noble gases.

In addition, off-site isotopic analysis of collected drilling fluid samples, specifically $\delta^{13}C$ and ^3He / ^4He, should be undertaken to explain the origin, evolution and migration pathways of these gases (Wiersberg and Erzinger, 2007). Such analyses can differentiate between biogenic and abiogenic sources, providing essential insights into the genetic models of gas occurrences in the Bushveld Complex. Hydrogeochemical samples must be collected during the Phase-3 surveying to facilitate data comparison with the findings in this article, thereby further ascertaining the potential for hydrothermal fluid migration through structural conduits.

Ultimately, the study addresses fundamental questions about the genesis and thermal evolution of the Bushveld Complex. Continued integration of geochemical, structural and isotopic tools will be essential for advancing the region's economic geology and assessing its geothermal potential.

Data availability. The BVDP project dataset is under moratorium, which will end in 2026, after which the public dataset will be published on the ICDP website (https://www.icdp-online.org/, last access: 18 February 2026).

Author contributions. RL: conceptualisation, data curation, field investigation, formal analysis, investigation, methodology, validation, visualisation, writing (original draft preparation, review and editing). AJA: data curation, formal analysis, funding acquisition, project administration, resources, supervision, writing. SSD: data curation, project administration, resources. FR: data curation, project administration, funding acquisition, resources. All of the co-authors contributed to the review and revision of the paper. All of the authors have read and agreed to the published version of the paper.

Competing interests. The contact author has declared that none of the authors has any competing interests.

Disclaimer. Publisher's note: Copernicus Publications remains neutral with regard to jurisdictional claims made in the text, published maps, institutional affiliations, or any other geographical representation in this paper. While Copernicus Publications makes every effort to include appropriate place names, the final responsibility lies with the authors. Views expressed in the text are those of the authors and do not necessarily reflect the views of the publisher.

Acknowledgements. The Water Research Commission is acknowledged for the funding of this project, without which none of this work would have been possible. Special thanks are extended to the ICDP-funded Bushveld Complex Drilling Project (BVDP) for facilitating the water research aspects related to the BVDP well, including the steering committee: Susan Webb, Stuart Hill, Robert Trumbull, Thulani Maupa, Lewis Ashwal and Reiner Klemd. Further gratitude is due to the technical staff at the drill site, Kwena Mathopa, Mabatho Mapiloko and Katlego Tlaila, as well as Pieter Frederik Grobler, for assisting on-site during data collection. Lore-Mari Deysel and the Institute for Groundwater Studies Laboratory are thanked for their collaboration on the water quality analysis of the collected water samples with drilling fluids. Janine Colling and Chris Harris from the BIOGRIP Laboratories are also recognised for their collaboration in analysing the collected water samples with drilling fluids for stable water isotopes. Marius Smit and Lorinda Rust are acknowledged for their support services at the Institute for Groundwater Studies (University of the Free State). Gratitude is expressed to Grammarly for its writing assistance tools, which contributed significantly to enhancing the grammar, clarity and coherence of the initial versions of this paper.

Financial support. This research has been supported by the Water Research Commission (grant nos. 2022/2023-00812 and ICDP-2019/04 (5067)).

Review statement. This paper was edited by Tomoaki Morishita and reviewed by Biswajit Ghosh and one anonymous referee.

References

Bilenker, L. D., VanTongeren, J. A., Lundstrom, C. C., and Simon, A. C.: Iron isotopic evolution during fractional crystallisation of the uppermost Bushveld Complex layered mafic intrusion, Geochem. Geophys. Geosy., 18, https://doi.org/10.1002/2016GC006660, 2017.

Boumaiza, L., Stotler, R., and Frape, S.: A review of the major chemical and isotopic characteristics of groundwater in crystalline rocks of the Canadian Shield, Chemical Geology, 669, 122366, https://doi.org/10.1016/j.chemgeo.2024.122366, 2024.

Brown, R. T.: A review of the origins of methane and its occurrences at the RPM Rustenburg section, ResearchGate, https://www.researchgate.net/publication/362391929_A_REVIEW_OF_THE_ORIGINS_OF_METHANE_AND_ITS_OCCURRENCE_AT_RPM_RUSTENBURG_SECTION (last access: 18 February 2026), 1992.

Cawthorn, R. G.: The Bushveld Complex, in: The Geology of South Africa, edite by: Johnson, M., Anhaeusser, C. R., and Thomas, R. J., Geological Society of South Africa Council for Geoscience Johannesburg, Pretoria, South Africa, ISBN 978-1-919908-77-9, 2006.

Cole, J., Finn, C. A., and Webb, S. J.: Deep magmatic chambers for crustal layered mafic intrusions: An example from the Bushveld Complex in southern Africa, Precambrian Research, 403, 107306, https://doi.org/10.1016/j.precamres.2024.107306, 2024.

Contreras, K., Nyblade, A., Durrheim, R., Webb, S., Manzi, M., and Fadel, I.: Crustal structure of the Bushveld complex, South Africa from 1D shear wave velocity models: Evidence

for complex-wide crustal modification, Tectonophysics, 890, 230496, https://doi.org/10.1016/j.tecto.2024.230496, 2024.

Cook, A. P.: Occurrence, emission and ignition of combustible strata gases in Witwatersrand gold mines and Bushveld platinum mines, and means of ameliorating related ignition and explosion hazards, part 1: literature and technical review, Safety in mines research advisory committee, GAP 504 (report), Itasca Africa (Pty) Ltd, ResearchSpace, https://researchspace.csir.co.za/server/api/core/bitstreams/6800a5bf-a399-4091-94da-c696120d1809/content (last access: 18 February 2026), 1998.

Cook, P.: Introduction of Isotopes and Environmental Tracers as Indicators of Groundwater Flow, The Groundwater Project, Guelph, Ontario, Canada, ISBN 978-1-7770541-8-2, 2020.

Craig, H. I.: Isotopic variations in meteoric water, Science, 113, 1702–1703, 1961.

Crow, H.L., Ladevèze, P., Laurencelle, M., Benoit, N., Rivard, C., and Lefebvre, R.: Downhole geophysical logging and preliminary analyses of bedrock structural data for groundwater applications in the Montérégie Est area, Québec, Geological Survey of Canada, Open File 7077, https://doi.org/10.4095/292295, 2013.

Curewitz, D. and Karson, J. A.: Structural settings of hydrothermal outflow: Fracture permeability maintained by fault propagation and interaction, Journal of Volcanology and Geothermal Research, 79, 149–168, 1997.

Daya, P.: The petrology and petrogenesis of lamprophyric dykes in the Bushveld Complex, and their possible role in causing gas outbursts, MSc thesis, University of the Witwatersrand, South Africa, 136 pp., WIReDSpace, https://wiredspace.wits.ac.za/server/api/core/bitstreams/9dfd7f92-f3b8-4aeb-a4fa-ccb0d24681bc/content (last access: 18 February 2026), 2019.

Durowoju, O. S.: Determination of isotopic composition of rainwater to generate local meteoric water line in Thohoyandou, Limpopo Province, South Africa, Water SA, 45, 183–189, https://doi.org/10.4314/wsa.v45i2.04, 2019.

Erzinger, J., Wiersberg, T., and Zimmer, M.: Real-time mud gas logging and sampling during drilling, Geofluids, 6, 225–233, https://doi.org/10.1111/j.1468-8123.2006.00152.x, 2006.

Forrest, M. J., Kulongoski, J. T., Edwards, M. S., Farrar, C. D., Belitz, K., and Norris, R. D.: Hydrothermal contamination of public supply wells in Napa and Sonoma Valleys, California, Applied Geochemistry, 33, 25–40, https://doi.org/10.1016/j.apgeochem.2013.01.012, 2013.

Freeze, R. A. and Cherry, J. A.: Groundwater, ISBN 0-13-365312-9, 1979.

Gebrekristos, R. and Cheshire, P.: Hydrogeological properties of the UG2 Pyroxenite aquifers of the Bushveld Complex, in: Proceedings of the 5th Platinum Conference of the Southern African Institute of Mining and Metallurgy, 143–152, https://www.platinum.org.za/Pt2012/Papers/143-152_Gebrekristos.pdf (last access: 18 February 2026), 2012.

Gudmundsson, A.: The propagation paths of fluid-driven fractures in layered and faulted rocks, Geological Magazine, 159, 1978–2001, https://doi.org/10.1017/S0016756822000826, 2022.

Harney, D. M. W. and Von Gruenewaldt, G.: Ore-forming processes in the upper part of the Bushveld complex, South Africa, Journal of African Earth Sciences, 20, 7789, https://doi.org/10.1016/0899-5362(95)00034-Q, 1995.

Hasan, M., Shang, Y., Shao, P., Yi, X., and Meng, H.: Geophysical research on rock mass quality evaluation for infrastructure design, Earth and Space Science, 9, https://doi.org/10.1029/2021EA002017, 2022.

Henry, G. and Brovko, F.: The Identification and Prediction of the Pressurised Gases in the Bushveld Complex Platinum, CSIR Centre for Mining Innovation, SIM 1304901, 72 pp., https://mhsc.org.za/sites/default/files/public/research_documents/SIM%20130401%20Report.pdf (last access: 18 February 2026), 2014.

Hughes, H. S. R., Kinnaird, J. A., McDonald, I., Nex, P. A. M., and Bybee, G. M.: Lamprophyric dykes in the Bushveld Complex: the lithospheric mantle and its metallogenic bearing on Bushveld large igneous province, Applied Earth Science, 125, 85–86, https://doi.org/10.1080/03717453.2016.1166638, 2016.

Krmíček, L. and Chalapathi Rao, N. V.: Lamprophyres, Lamproites and Related Rocks: Tracers to Supercontinent Cycles and Metallogenesis, Geological Society, London, Special Publications, 513, 1–16, https://doi.org/10.1144/sp513-2021-159, 2022.

Kumar, P. J. S.: Interpretation of groundwater chemistry using piper and chadha's diagrams: a comparative study from perambalur taluk, Elixir Geoscience, 54, 12208–12211, 2013.

Liu, J., Wu, H., Zhang, F., Liu, S., Liu, Z., and Yan, H.: Improvement in the method for borehole caliper measurement based on azimuthal gamma-gamma density well logging, Applied Radiation and Isotopes, 145, 68–72, https://doi.org/10.1016/j.apradiso.2018.12.014, 2019.

Marsh, J. S., Pasecznyk, M. J., and Boudreau, A. E.: Formation of Chromitite Seams and Associated Anorthosite in Layered Intrusions by Reactive Volatile-rich Fluid Infiltration, Journal of Petrology, 62, 1–23, https://doi.org/10.1093/petrology/egaa109, 2021.

Montone, P., Pierdominici, S., Mariucci, M. T., Mirabella, F., Urbani, M., Akimbekova, A., Chiaraluce, L., Johnson, W., and Barchi, M. R.: Geophysical downhole logging analysis within the shallow-depth ICDP STAR drilling project (central Italy), Solid Earth, 15, 1385–1406, https://doi.org/10.5194/se-15-1385-2024, 2024.

Mouat, A. P., Siegel, Z. A., and Kaiser, J.: Evaluation of Aeris mid-infrared absorption (MIRA), Picarro CRDS (cavity ring-down spectroscopy) G2307, and dinitrophenylhydrazine (DNPH)-based sampling for long-term formaldehyde monitoring efforts, Atmos. Meas. Tech., 17, 1979–1994, https://doi.org/10.5194/amt-17-1979-2024, 2024.

Muccio, Z. and Jackson, G. P.: Isotope ratio mass spectrometry, The Royal Society of Chemistry, Analyst, 134, 213–222, https://doi.org/10.1039/B808232D, 2009.

Ortega, L. and Gil, L.: Isotope hydrology; an overview, IAEA Bulletin, 4–5, https://gordonfoundation.ca/wp-content/uploads/2023/04/6010405_corr.pdf (last access: 18 February 2026), 2019.

Pohl, W. L.: Economic Geology Principles and Practice. Metals, Minerals, Coal and Hydrocarbons – Introduction to Formation and Sustainable Exploitation of Mineral Deposits, Wiley-Blackwell, ISBN 9781444336627, 2011.

Scoon, R. and Viljoen, M.: The Eastern limb of the Bushveld Complex, South Africa, Africa's Top Geological Sites, 35th International Geological Congress in Cape Town, Cape Town, South

Africa, Struik Nature, a division of Penguin Random House (Pty) Ltd, ISBN 978-1-7758-448-8, 2016.

Setera, J. B., VanTongeren, J. A., Turrin, B. D., and Swisher III, C. C.: A low-temperature hydrothermal cut off: plagioclase ^{40}Ar / ^{39}Ar thermochronology of the Rustenburg Layered Suite, Bushveld Complex, Contributions to Mineralogy and Petrology, 178, https://doi.org/10.1007/s00410-022-01984-9, 2023.

Sherwood Lollar, B., Lacrampe-Couloume, G., Slater, G. F., Ward, J., Moser, D. P., Gihring, T. M., Lin, L.-H., and Onstott, T. C.: Unravelling abiogenic and biogenic sources of methane in the Earth's deep surface, Chemical Geology, 266, 328–339, https://doi.org/10.1016/j.chemgeo.2005.09.027, 2006.

Skursch, O., Tegner, C., Barfod, G. H., Andreasen, R., and Lesher, C. E.: Granites and Granophyres of the Bushveld Complex, South Africa: A review, Earth-Science Reviews, 250, 104703, https://doi.org/10.1016/j.earscirev.2024.104703, 2024.

Stemprok, M. and Seifert, T.: An overview of the association between lamprophyric intrusions and rare metal mineralisation, Mineralogia, 42, 121–162, https://doi.org/10.2478/v10002-011-0011-x, 2011.

Titus, R., Witthüser, K., and Walters, B.: Groundwater and mining in the Bushveld Complex, in: Proceedings of the International Mine Water Conference, Pretoria, South Africa, 19–23 October 2009, 178–184, ISBN 978-0-9802623-5-3, 2009.

Vonopartis, L., Nex, P., Kinnaird, J., and Robb, L.: Evaluating the Changes from Endogranitic Magmatic to Magmatic-Hydrothermal Mineralization: The Zaaiplaats Tin Granites, Bushveld Igneous Complex, South Africa, Minerals, 10, 379, https://doi.org/10.3390/min10040379, 2020.

Wedge, D., Holden, E.-J., Dentith, M., and Spadaccini, N.: Fast and objective detection and analysis of structures in downhole images, Journal of Applied Geophysics, 144, 157–172, https://doi.org/10.1016/j.jappgeo.2017.07.004, 2017.

Wiersberg, T. and Erzinger, J.: A helium isotope cross-section study through the San Andreas Fault at seismogenic depths, Geochem. Geophys. Geosy., 8, https://doi.org/10.1029/2006GC001388, 2007.

Zaccarini, F. and Garuti, G.: Zoned Laurite from the Merensky Reef, Bushveld Complex, South Africa: "Hydrothermal" in Origin?, Minerals, 10, 373, https://doi.org/10.3390/min10040373, 2020.

Zeh, A., Ovtcharova, M. Wilson, A. H., and Schaltegger, U.: The Bushveld Complex was emplaced and cooled in less than one million years – results of zirconology and geotectonic implications, Earth and Planetary Science Letters, 418, 103–114, https://doi.org/10.1016/j.epsl.2015.02.035, 2015.

Zhitova, L. M., Kinnaird, J. A., Gora, M. P., and Shevko, E. P.: Magmatogene Fluids of Metal-Bearing Reefs in the Bushveld Complex, South Africa: Based on Research Data on Fluid Inclusions in Quartz, Geology of Ore Deposits, 58, 58–81, https://doi.org/10.1134/S1075701515050086, 2016.

Zhou, H., Trumbull, R. B., Veksler, I. V., and Bachmann, K.: The effects of iron-rich ultramafic pegmatite on the composition and mineralogy of the UG2 chromitite: a case study in the western Bushveld Complex, South Africa, Mineralium Deposita, 58, 1005–1021, https://doi.org/10.1007/s00126-023-01167-x, 2023.

Zientek, M. L., Causey, J. D., Parks, H. L., and Miller, R. J.: Platinum-group elements in southern Africa: Mineral inventory and an assessment of undiscovered mineral resources, U.S. Geological Survey Scientific Investigation Report, 2010-5090-Q, 126, https://doi.org/10.3133/sir20105090Q, 2014.